# High-Voltage Bias-Switching Electronics for Volumetric Imaging Using Electrostrictive Row–Column Arrays

Afshin Kashani Ilkhechi, *Member, IEEE*, Randy Palamar, *Graduate Student Member, IEEE*,
Mohammad Rahim Sobhani, *Student Member, IEEE*,
Darren Dahunsi, *Graduate Student Member, IEEE*, Christopher Ceroici, *Member, IEEE*,
Mahyar Ghavami, *Student Member, IEEE*,
Jeremy Brown, *Member, IEEE*, and Roger Zemp, *Member, IEEE*

Abstract—**Top orthogonal to bottom electrode (TOBE) arrays, also known as row–column arrays, hold great promise for fast high-quality volumetric imaging. Bias-voltage-sensitive TOBE arrays based on electrostrictive relaxors or micromachined ultrasound transducers can enable readout from every element of the array using only row and column addressing. However, these transducers require fast bias-switching electronics which are not part of a conventional ultrasound system and are nontrivial. Here we report on the first modular bias-switching electronics enabling transmit, receive, and biasing on every row and every column of TOBE arrays, supporting up to 1024 channels. We demonstrate the performance of these arrays by connection to a transducer testing interface board (IB) and demonstrate 3-D structural imaging of tissue and 3-D power Doppler imaging of phantoms with real-time B-scan imaging and reconstruction rates. Our developed electronics enable interfacing of bias-switchable TOBE arrays to channel-domain ultrasound platforms with software-defined reconstruction for next-generation 3-D imaging at unprecedented scales and imaging rates.**

Index Terms— **2-D arrays, 3-D ultrasound, synthetic aperture imaging, ultrasound electronics.**
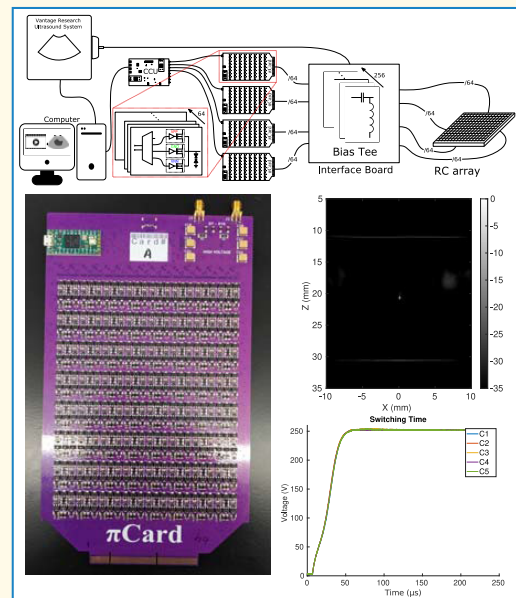
I. Introduction and Background

THREE-dimensional ultrasound imaging holds great promise for preclinical and clinical ultrasound [1], [2].

Afshin Kashani Ilkhechi, Randy Palamar, Mohammad Rahim Sobhani, Darren Dahunsi, Christopher Ceroici, Mahyar Ghavami, and Roger Zemp are with the Department of Electrical and Computer Engineering, University of Alberta, Edmonton, AB T6G 2R3, Canada (e-mail: mahyar.ghavami@ualberta.ca; rzemp@ualberta.ca).
Jeremy Brown is with the School of Biomedical Engineering, Dalhousie University, Halifax, NS B3H 1V7, Canada.

However, no commercial 2-D arrays exist for high-frame-rate preclinical imaging applications, and 3-D ultrasound in clinical domains is not always preferred over more conventional 2-D B-scan imaging. This in part may be due to sacrificed image quality owing to engineering tradeoffs in 2-D arrays [3]. Wiring becomes unwieldy for fully connected 2-D arrays with large channel counts. Matrix probes with integrated micro-beamformers represent the state-of-the-art but these use beamforming approximations that can result in degraded in-plane performance [4], [5], [6], [7]. Moreover, these Matrix probes are complex, may require active cooling, are not easily scalable, and are not yet capable of advanced ultrafast imaging modes. Several strategies have been proposed to reduce the complexity of fully wired arrays including sparse-array architectures [8]. However, sparse arrays are not readily scalable for large arrays important for high-numerical aperture high-quality wide-field-of-view imaging. Moreover, image quality in sparse arrays is sacrificed compared to fully wired arrays [9], [10], [11], [12], [13].

Highlights

- **This paper describes the implementation of 256 channel high voltage biasing electronics for use with electrostrictive relaxor based ultrasound transducer arrays.**

- **Bi-polar voltages up to ±250V are delivered in approximately 100 μs and this is used to perform cross-plane FORCES and Power Doppler imaging in real-time.**

- **The demonstrated electronics provide a basis for future work implementing complex bias encoded imaging schemes with novel bias-sensitive row column ultrasound arrays.**

Row–column arrays, originally introduced by the Lockwood group in [14], hold great promise for high-quality 3-D imaging as they require only row and column addressing [15]. However, these are only capable of transmit focusing in elevation and receive focusing in azimuth (or vice versa) rather than both transmit and receive focusing in plane as is the case with more conventional B-scan imaging with a linear array transducer.

We introduced bias-switchable row–column arrays, also known as top-orthogonal to bottom electrode (TOBE) arrays, based on CMUTs or electrostrictive relaxors [16], [17], [18]. Fig. 1 gives an example of one such array constructed with an electrostrictive relaxor. These differ from the original piezoelectric row–column arrays in that elements are not active unless a bias voltage is applied. The addition of bias voltages enables new opportunities that could not be achieved with more conventional piezoelectric row–column arrays. For example, we demonstrated that it could be possible to read out from every element of the TOBE array using bias-voltage aperture encoding [9], [18], [19]. This was not previously possible with piezoelectric TOBE arrays. While it was conjectured that single-element actuation could be achieved by biasing one column of a piezoelectric row–column array and leaving the others floating, then transmitting on a row, in practice, capacitive coupling of RF signals created a complex and unwanted excitation not localized to a desired row–column element. In contrast, in our approach, we used CMUTs or electrostrictive relaxors rather than piezoelectric materials to create TOBE arrays.

An electrostrictive material is not inherently piezoelectric until a bias voltage is applied, and the induced polarity is bias-voltage dependent [20], [21]. Thus, by biasing a column, while grounding all others, and transmitting along a row, single element actuation was achieved. Since ac-coupled signals are grounded rather than floating, unwanted RF crosstalk between rows and columns is mitigated. Similarly, by biasing a column, and grounding all others, then receiving on rows, we can activate an effective linear array of elements that can be electronically stepped across a 2-D aperture [17]. This is one means of reading out from every element of a bias-switchable TOBE array.

More complicated imaging sequences can be achieved using a superposition of single transmit or single-receive element principles. In particular, we previously demonstrated enhanced signal-to-noise-ratio 3-D photoacoustic imaging using Hadamard aperture bias encoding [19]. So-called simultaneous azimuth and Fresnel elevational (SAFE) compounding was demonstrated for high-quality B-scan imaging with good
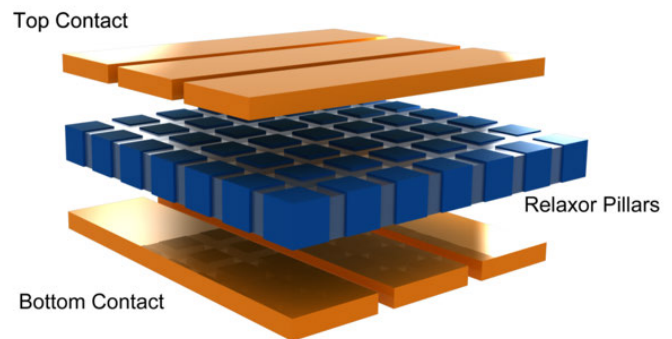

Fig. 1. Illustration of an electrostrictive relaxor TOBE array.

elevational focusing based on a binary Fresnel Lens concept. We further demonstrated a technique called fast orthogonal row–column electronic scanning (FORCES) that used bias encoding of TOBE arrays to achieve aperture-encoded synthetic aperture imaging in azimuth while achieving transmit focusing on elevation [9].

These and future bias-encoded imaging strategies required a means of switching bias voltages on rows and columns, a functionality absent in conventional ultrasound systems. Our early prototypes used relay boards to accomplish this task. However, mechanical relays have slow switching speeds and further created current surges that could cause arcing which could damage electronics and arrays. In SAFE compounding, transmitting and receiving electronics were on rows while biasing electronics were applied to columns. However, in FORCES imaging, transmission was on rows but biasing and reception were on columns. For cross-plane imaging, the roles of rows and columns are reversed.

In cross-plane FORCES and in future imaging methods, it will be important to offer biasing, transmitting, and reception on each row and each column of a TOBE array. However, solid-state electronics for achieving this have not yet been achieved. Additionally, previous bias-switching electronics were limited to voltages of 50 V for switching $\geq$10 MHz electrostrictive arrays. For lower frequency diagnostic electrostrictive arrays important for clinical applications, a thicker transducer will be required to achieve these lower frequencies. As such, a higher bias voltage will be needed to achieve the same electric field for biasing. Additionally, some CMUT arrays require higher bias voltages (e.g., over 100 V) for optimal operation [22], [23].

We sought to develop modular and programmable high-voltage and fast bias-switching boards that could enable
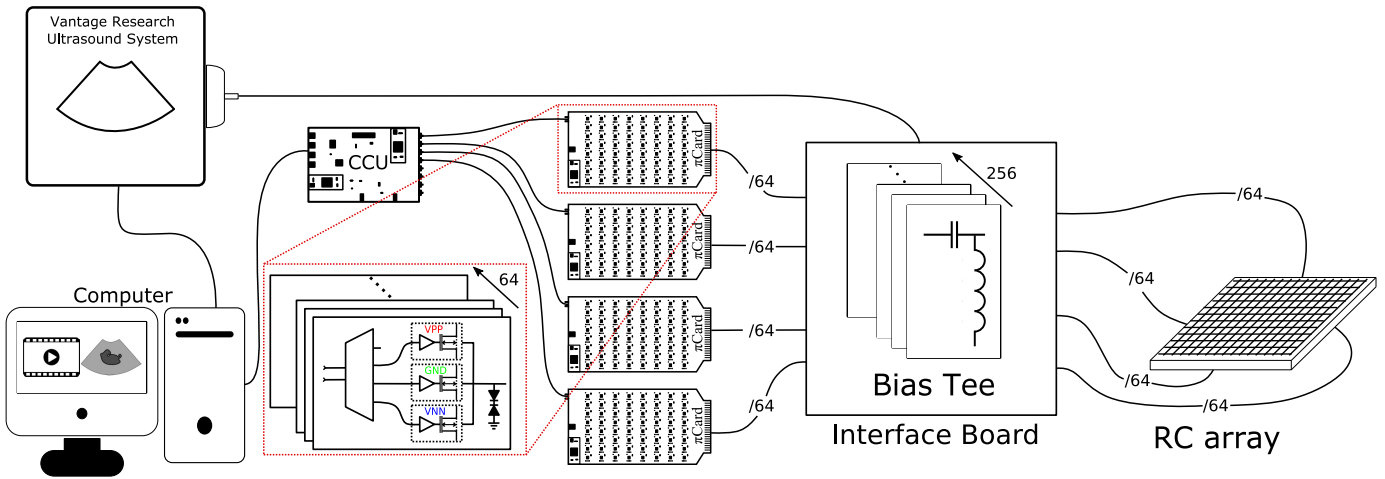
Fig. 2. Block diagram of bias-controlled ultrasound imaging system. The inset shows a simplified representation of a πCard's functionality. Each πCard contains 64 channels and each channel produces 1 of 4 states. These states are given in Table II.

interfacing a bias-switchable row–column probe to a Verasonics Vantage ultrasound platform or other research ultrasound platforms. Bias voltages up to ± 250 V, sufficient for most clinical and preclinical applications, were needed. In addition to the high bias voltages, switching times in the microseconds are required to enable ultrafast imaging modes. These requirements are difficult to implement, especially given that the electronics need to withstand high bias voltages while carrying high transmit voltage pulses. These and other challenges will be further elaborated upon.

We developed high-voltage bias-switching electronics using high-voltage MOSFETs in a modified H-bridge architecture. The boards are modular and programmable supporting up to 1024 channels. Example TOBE arrays are tested on an interfacing board, demonstrating 3-D Power Doppler imaging of phantoms, and 3-D tissue imaging.

II. METHODS

The proposed bias-switching and interfacing electronics aim to meet the following specifications.

1) Every channel in the imaging system should be connected to biasing, pulsing, and receiving electronics simultaneously to provide flexibility for the imaging schemes executed using the row–column arrays.
2) High-voltage handling is required. To permit certain imaging schemes, the electronics should be designed to accommodate a high bias voltage in combination with a high transmit pulse. For example, for some imaging schemes, high transmit pulses are needed to perform deep-tissue imaging. These transmit pulses can be as high as 200 V peak-to-peak or more. Such high transmit voltages and associated large peak currents in combination with high bias voltages can damage many solid-state components.
3) Biasing electronics should provide enough current for the electrostrictive material (or CMUTs) to change their polarity. In our work, switching 128 channels simultaneously from 0 to 250 V requires nearly 2 A of peak current. Imaging schemes that involve high transmit pulsing and fast bias switching may also produce transient peak current that may damage electronics if not accounted for.

4) Biasing electronics should perform fast bias switching within a time scale of approximately 100 μs. To achieve imaging depths useful for medical imaging purposes while using fast bias-voltage switching to increase image-capturing speeds, high bias-voltages with fast switching times are needed. However, if the switching time is too fast, unwanted acoustic transients could be created. To minimize this effect, while ensuring switching can be done as fast as possible to achieve high frame rates, we chose the switching time to be longer than the reciprocal of the transducer bandwidth, but shorter than the pulse-echo transit time. Targeting 1–15 MHz diagnostic frequencies, and imaging depths of 15 cm or more, we require switching times longer than a few μs but shorter than about 100 μs.
5) Biasing electronics should provide bias voltages as high as ± 250 V. As noted herein, bias-switchable arrays intended for diagnostic frequencies (i.e., with center frequencies <20 MHz) may require high bias voltages for high electromechanical efficiency. Some lower diagnostic frequencies, such as the 2–3 MHz commonly used in cardiac probes, require a thick electrostrictive layer and thus a large bias voltage to achieve the internal electric field needed for polarization; however, thinner arrays used for higher frequencies will not require such high bias voltages. For example, a 2 MHz array may require ± 250 V for biasing, whereas a much thinner 10 MHz array may only require ± 50 V.
6) Finally, the biasing system should have modular units to accommodate various output channel requirements based on the transducer specifications. For example, in an imaging system utilizing TOBE arrays with 128×128 elements, biasing electronics must provide 256 programmable channels, while an array with 512×512 elements will require 1024 channels.

These design requirements are summarized in Table I.

A. Technical Challenges

In various iterations of previous designs, we used off-the-shelf high-voltage multiplexer ICs that could switch between VPP, VNN, and ground for each channel. However, these ICs

TABLE I
BIAS-SWITCHING ELECTRONICS IDEAL REQUIREMENTS

Parameter	Requirement
Bias Voltage Swing	± 250V
Transmit Voltage on top of Bias	190Vpp
Channel Count	256 for 128x128 TOBE array
Switching Time	$0.5\mu s < t_s < 100\mu s$
Total Peak Current	$\approx$ 2A for 128 channels
Peak Current per Channel	$\approx$ 16mA

TABLE II
πCARD CHANNEL STATES

State	Output
1	High Impedance (>100GΩ)
2	V_{nn} (Down to -500V)
3	V_{pp} (Up to 500V)
4	DC GND

were only designed for bias voltages of ± 100 V, not including over-voltages due to transmit pulses. When testing only a single channel, some test circuits behaved well, but when connected to 256 channels and all channels were transmitting, the high-voltage MUX ICs were damaged. Additionally, low-level CMOS and TTL logic including shift-registers used for bias control and timing would end up scrambled after ultrasound transmit pulses.

To mitigate these problems, our new design used high-voltage MOSFETs rated to ± 500 V. Additionally, a four-layer PCB was used with low-voltage logic situated on one side and high-voltage components situated on the opposite side. To further minimize logic scrambling and communication problems between the boards and the host PC, we opted to use well-shielded USB-C cables and error checking.

Other flaws of previous designs included insufficient peak current to enable fast high-voltage switching. To remedy this problem, we designed a custom central control unit (CCU) board powered by a power supply capable of delivering both high voltages and peak currents. Voltage droop during switching or transmit events was minimized using reservoir capacitors on VPP and VNN power bus lines.

Another problem unique to bias-switchable row–column arrays is the danger of having array electrodes that are shorted because of fabrication imperfections. The danger is that if a high positive voltage is applied to a first column, but the adjacent column is shorted to this first column and a negative or ground voltage is applied, it will create a large current through the shorted connection resulting in damaged electronics and/or arrays, even with a single shorted channel. Thus, it was imperative to offer a utility to map shorted or dead channels for each array and to offer a high-impedance state for shorted elements.

B. New Design for High-Voltage Bias Electronics

Fig. 2 provides an overview of the proposed imaging system. The biasing system (which we call a πCard system named

for the H-bridge architecture which looks like a π-symbol) consists of three main units.

1) The interface board (IB) consists of individual bias tees to combine ac and dc signals and deliver them to TOBE arrays.
2) The biasing boards (πCards) consist of 64 independent programmable high-voltage channels. Every channel can be programmed to one of four electrical states, given in Table II, at any time.
3) The CCU, which is the main hub to communicate with the imaging system including the host computer, ultrasound imaging system, πCards, and high-voltage power supplies.

In the following subsections, each unit is described in more detail:

1) Interface Board: The IB provides a bridge between the imaging system and an ultrasound transducer array. The board makes it convenient to connect transducer array prototypes and includes per-channel bias-tees for coupling ac ultrasound signals onto dc bias voltages. Fig. 3(a) shows the IB. ac inputs are brought onto the board through 40-pin micro-coax connectors (I-PEX). A custom ZIF-connector was fabricated for connecting the ultrasound platform to the IB. πCards can be connected to the IB through four board-to-board connectors positioned at the bottom side of the IB. Prototype transducer PCBs (SURF boards) can be mounted to the IB. Fig. 3(b) shows the IB with all the connections.

2) Bias-Switching Cards (πCards): The πCards are designed to receive biasing instructions in advance and execute bias voltage switching patterns during an ultrasound or photoacoustic imaging pulse sequence.

Every channel on a πCard can be programmed at any point in the pulse sequence to one of the four supported states given in Table II. All channels have a circuit block for generating each of the available states. Fig. 4 shows one such circuit block for generating VPP on a single channel. The circuit can be divided into two sections: a gate driver and a switching transistor. The comparator A1 is essential in preventing unwanted triggers caused by high electric fields and noise during imaging. In contrast to switching electronics where transitions need to be made as fast as possible, the πCards are designed to gradually ramp the output voltage. This gives the material enough time to respond without causing an undesired transmit.

Fig. 5(a) illustrates a scenario where a single element of a TOBE array is biased at VPP and Fig. 5(b) shows the voltage transition on several channels of a πCard with an array connected. Starting from GND the πCard gradually transitions the channel's output toward VPP.

The slew rate for the MOSFETs is mostly determined by the gate current which is in part determined by resistors $R3$ and $R4$ shown in Fig. 6. A theoretical analysis of this is quite involved and beyond the scope of this article. Since the full circuit's output slew rate is not fixed due to variable load and bias voltages, we tried to profile the unloaded slew rate with experimental measurements. This was not done in SPICE due to a lack of available models for the selected MOSFETs.
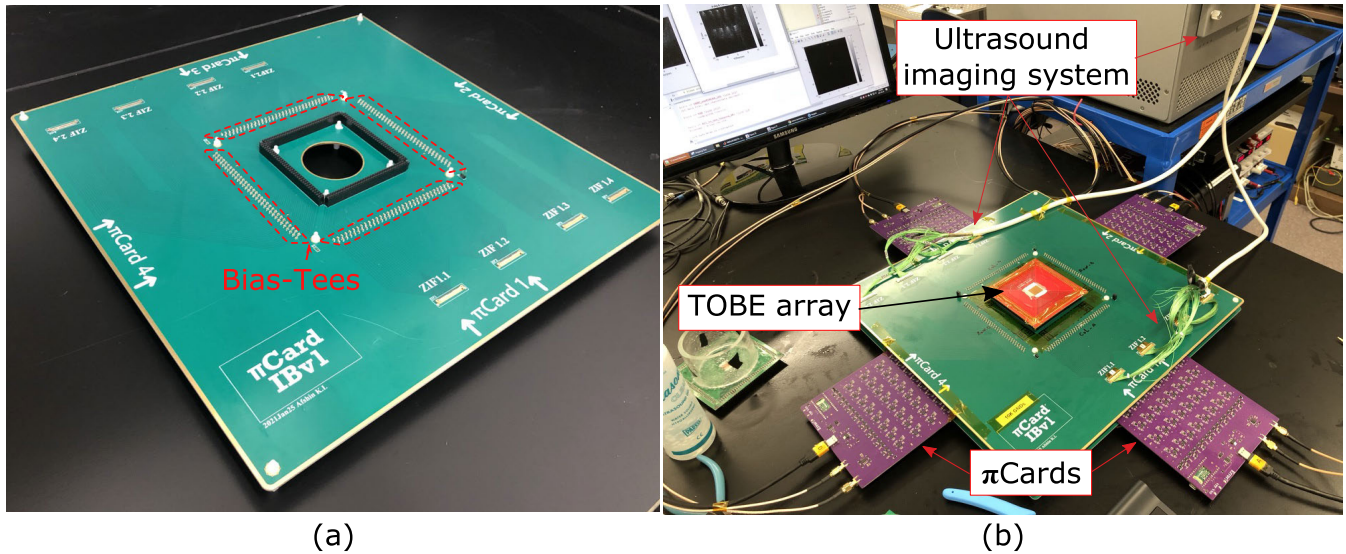
Fig. 3. IB to connect πCards and Verasonics. (a) Unconnected IB. The board has 256 individual bias-tees to support up to 256 imaging channels. (b) Ultrasound imaging setup. A 128 × 128 TOBE array SURF board is plugged into the designated area at the center of the IB. Four πCards are plugged into the IB for providing the bias voltages. A Verasonics vantage ultrasound imaging system is attached to the board through I-PEX connectors.
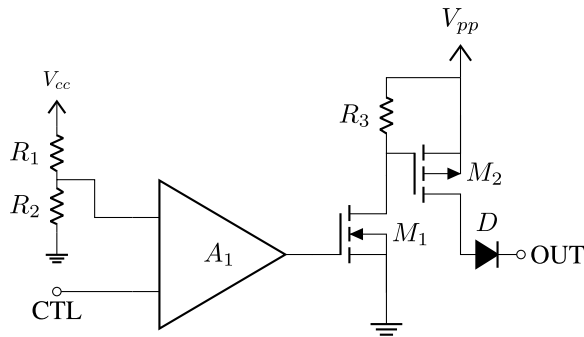

Fig. 4. Simplified block diagram of the VPP switching block.

We carried out measurements by placing various values for $R3$ and $R4$ and measuring the switching time of M2. Some of the design boundaries considered are as follows.

1) Maximum current flows through $R3$ and $R4$ when M2 is ON and should be limited (<1 mA).
2) M2's VGS needs to be limited to a nondestructive value (<20 V).
3) Maximum drain current to the load should be limited (<2 A).

To describe the effect of $R3$ and $R4$ on the slew rate we can consider two scenarios, one when M2 is OFF or turning ON and one when M2 is fully ON. When the transistor is turning on, the gate requires current and can be modeled as a low resistance resistor in parallel to $R4$, therefore, current passing through $R3$ will mostly go to the gate of M2. Here the current flowing into the gate is estimated with VGS/$R3$. For VPP levels such that the voltage created by the $R3$ and $R4$ voltage divider exceeds the 10 V Zener voltage, VGS will be clamped to 10 V. In the second scenario where M2 is ON, the gate no longer needs current and can therefore be modeled as a large resistor parallel to $R4$. Here the current to keep M2 ON will be determined by VPP/($R3+R4$). By considering

the two scenarios, and experimental measurements, a suitable range for $R3$ and $R4$ is determined. We kept the $R4/R3$ ratio fixed at 10 and tried values of $R3$ between 10 and 100 kΩ with a corresponding $R4$ in the range of 100 kΩ–1 MΩ.

After testing with our selected resistors ($R3 = 51$ kΩ, $R4 = 510$ kΩ), we concluded that the unloaded slew rate of the circuit was 107.5 V/μs. As a final note, parasitic capacitance in the PCB was neglected since it is small and our switching speed is also small. PCB traces widths were selected such that the trace resistance exceeded the requirements in IPC-2221B PCB standard [24] for the currents outlined earlier.

A head-to-head diode pair shown on the right of Fig. 6 is used in parallel with the output to provide a high-impedance state when all three blocks are disabled. The high-impedance state works based on the nonideal operations of diodes. Since diodes are placed head-to-head, at any point, one of the diodes will be in the reverse mode, allowing a minimal leakage current (in this case fA) to pass. Thus, diodes will allow only a negligible constant current to pass, almost independent of the bias voltage. This high-impedance state is used to prevent damage to the biasing electronics when an error in transducer manufacturing has left some channels shorted. Before use, a mapping procedure is performed to find and disable these shorted channels.

Note that a PFET is used to drive the output to VPP, shown in Figs. 4 and 6 while an NFET is used to drive the output to VNN. This keeps the circuit simple since the gate voltage for each of these devices can be derived directly from their respective source voltages.

The 10 V Zener diode Dz shown in Fig. 6 ensures that M2 does not fail from the source–gate voltage exceeding its breakdown voltage during a switching event.

While the VPP and VNN circuits can quickly drive the bias voltage to a high VPP or VNN value, we also need a method to quickly drive the channel to ground. This is accomplished using the circuit in Fig. 7, which contains both NFETS and
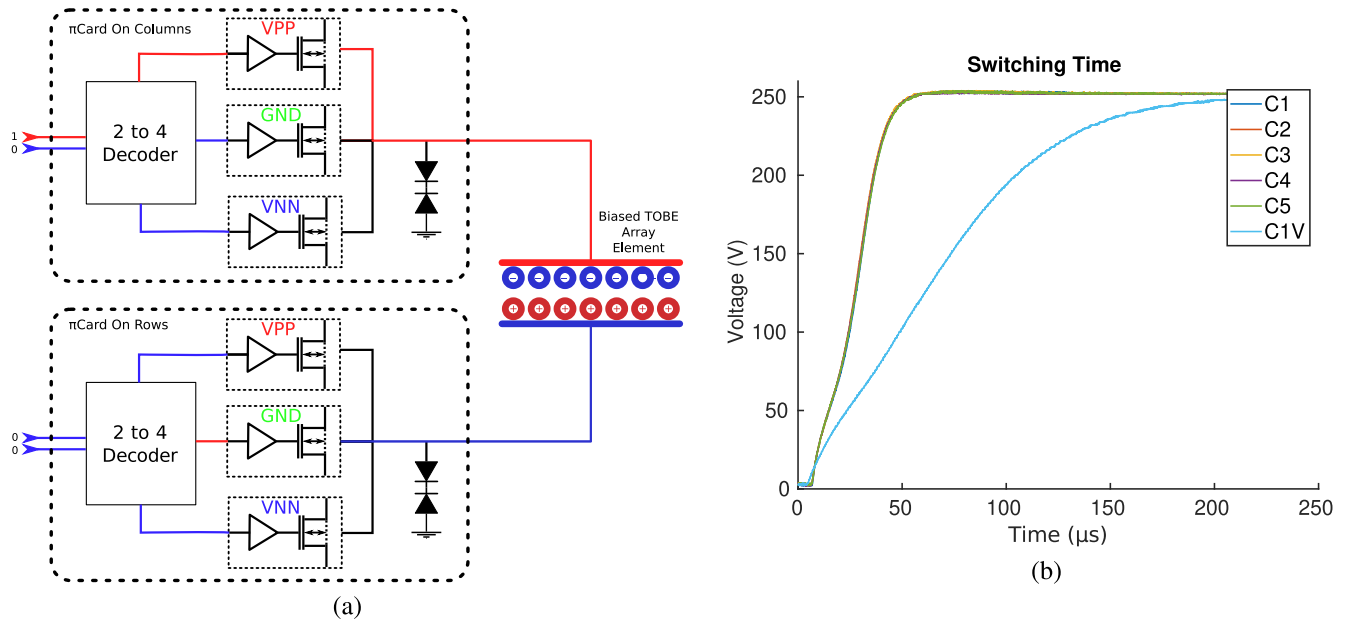
Fig. 5. (a) Block diagram of a single element of TOBE array biased with πCards. In this example, an electrostrictive TOBE array is connected to the πCards, where a column is biased with VPP and a row is biased GND. (b) Transitioning the output of a single channel from GND to VPP in 32.6 μs. C1V is the switching time with the Verasonics connected. This curve has a switching time of 118.5 μs.

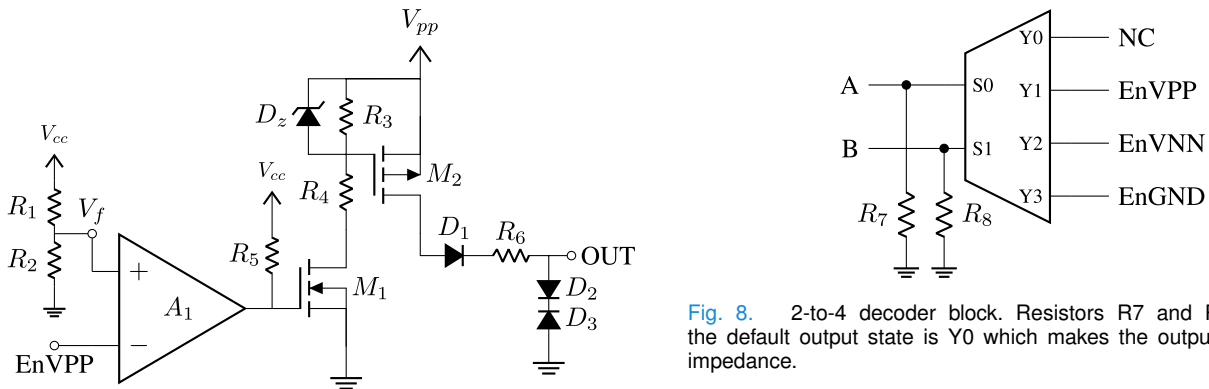Fig. 6. Full VPP switching circuit schematic.
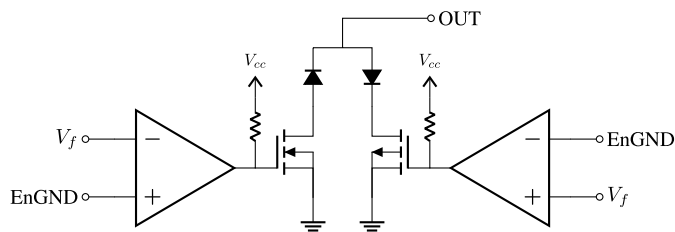
Fig. 7. Ground driving circuit schematic.

Fig. 8. 2-to-4 decoder block. Resistors R7 and R8 ensure that the default output state is Y0 which makes the output act as a high impedance.

PFETs to drive signals from a high-positive or high-negative voltage to ground faster than is possible with passive recovery.

Note that NFETS switch much faster than PFETs. This presents a problem. A VPP switching time different than the VNN switching time could result in shorting, resulting in high transient currents. To minimize this risk, FETs from the same manufacturer and device family were utilized in these circuits. Additionally, we needed to ensure that the transistors could withstand the current drawn by any shorted transducer channels caused by manufacturing errors. In the worst case, when a transducer is shorted to ground, 250 VDC will be dropped across $R6$, shown in Fig. 6. With $R6 = 10$ kΩ this current will be 25 mA. To support this, our chosen MOSFETs are rate to supply up to 100 mA (pulsed) with VDS at 250 VDC. The parasitic capacitance introduced by the MOSFETs was ignored since it is negligible in comparison to the bias tees and capacitance presented by the transducers.

When turning on VPP on all 256 channels, there may be a large rush current of Amps. There will thus be a tradeoff between switching speed and the current consumed.

The PLH250/-P dc Power Supply (Aim-TTi, U.K.) can supply up to 375 mA of current at 250 V. Capacitor banks in the CCU's (discussed below) power regulator circuits are used to ensure transient current draws above this current limit can be met.

In the full switching circuit shown in Fig. 6, $R5$ is a pull-up resistor for the comparator. This speeds up the switching time of M1 at the expense of increased power draw when the line is low. The differential comparator inputs prevent accidental switching due to noise generated by the high-voltage transmit

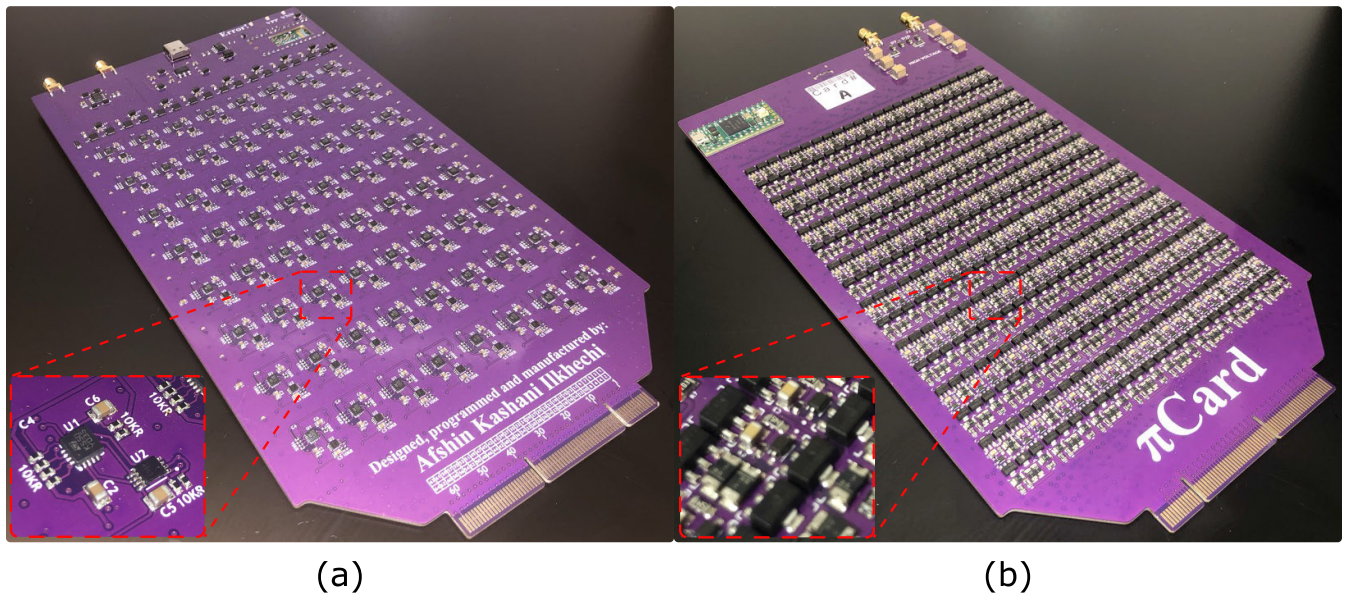Fig. 9.   Assembled πCards. (a) Logic side, consisting low-voltage electronics and logic controls. (b) High-voltage side, consisting high-voltage MOSFETs, and gate drivers.

pulses. The selected comparators can switch in <300 ns, which is negligible compared to our target switching times (<100 μs).

The 2 to 4 decoder shown in Fig. 8 and in block-form in Fig. 5 controls the output state blocks and provides two benefits: they reduce the digital control lines per channel from 3 to 2 and they prevent simultaneous activation of multiple output states. For example, two power supplies might be shorted if VPP and VNN blocks are activated simultaneously due to a software error or hardware glitch. However, since only one output of the decoder can be activated at any given time this is prevented. $R7$ and $R8$ ensure that the default state when the boards are first powered on and when lines A and B are not set is $Y0$, acting as a high-impedance state since all output blocks are disabled.

Serial-in, parallel-out shift register banks are used to write bias patterns to the bias-switching circuits on the πCards. A microcontroller on each πCard and on a CCU (discussed below) manages communication from the computer through the CCU to the πCards.

The shift registers contain clock, latch, enable, and reset lines. Data are clocked into the shift registers then pairs of data bits are sent in parallel to the 2-to-4 decoders. Bias voltages are switched when the latch line is pulsed high.

Switching the enable line high disables the shift registers and turns every channel into a high-impedance state. The CCU monitors for shorts or other problems. If these occur, the CCU turns the enable line high.

A bias pattern for 256 channels can be written to the shift registers every 1.6 μs.

Fig. 9 shows the two sides of a fabricated πCard where every πCard has been designed with 64 channels. Fig. 9(a) illustrates the logic side, including all digital electronics and low-voltage components, and Fig. 9(b) illustrates the high-voltage side of the board. Designing the board with separated low- and high-voltage sides helps to shield the sensitive electronics from high-voltage transients generated by the transistors.

3) Central Control Unit: The CCU is the main hub of our imaging system. It connects with the computer to receive biasing instructions and transfers them to the πCards. The CCU also synchronizes the πCards with the imaging system by generating trigger signals. Fig. 2 illustrates the CCU board with all the connections, and Fig. 10 shows a photograph of the fabricated CCU unit.

The CCU has the following inputs and outputs: Four USB-C ports route to four 64-channel πCards for biasing control. A PC USB connection is used to connect to the Verasonics Vantage system. Eight SMA ports are used as power bus lines to route VPP and VNN power to πCards.

±6 V is provided to the board for powering low-voltage components and voltages with a 500 Vpp range are supplied for the high-voltage components.

The board also has eight trigger outputs used for synchronization between circuits. Only two trigger lines (TrI1 and IO4) are needed for ultrasound imaging. Others can be used for photoacoustic imaging or other modalities.

TrI1 is a trigger input receiving triggers from the Verasonics. IO4 is used as a trigger output sending triggers to the Verasonics system. The Verasonics platform sends a trigger event to CCU then the CCU generates a trigger back to Verasonics system with a software-defined delay (for example to permit bias pattern write time) for a transmit event. Bias patterns can be sent to πCard micro-controllers for a whole imaging sequence (not only for each Tx event). Custom software was written to write biasing and control sequences from within the Verasonics pulse-sequence code.

The CCU has two main controllers, one handling the low-priority tasks such as communicating with the computer and the other controller to generate extremely precise control signals with a jitter of shorter than 1.6 ns to keep all the imaging units in sync.
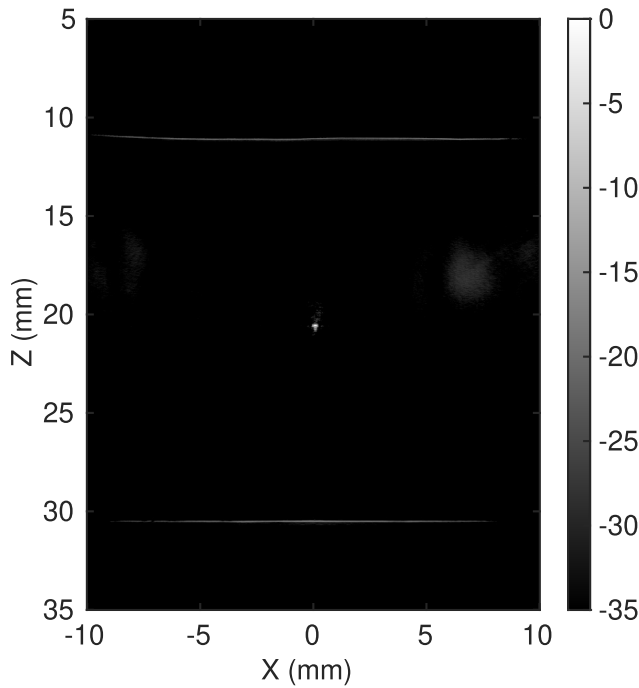
Fig. 10. CCU, the main hub of the imaging system. CCU can connect to power supplies, ultrasound imaging system, πCards, lasers, photodiodes, and a computer to synchronize all units for ultrasound and photoacoustic imaging.

The CCU is mainly responsible for regulating and supplying VPP and VNN voltages to the πCards. It is equipped with two 1 mF capacitor banks rated for 500 VDC to store energy and provide it during the transition times. The capacitor banks have equivalent series resistance (ESR) of 10 $\mu\Omega$. Low ESR is crucial for keeping the VPP and VNN voltages steady during the transition times where πCards may require a large transient current. The CCU is equipped with VPP and VNN monitoring circuits. These consist of voltage dividers and buffer amplifiers, where the output read voltages have opposition Zener diodes to ensure that read voltages do not exceed a threshold. The read voltages are monitored using an analog-to-digital converter. The CCU microcontroller may also query the power supplies to monitor current. VPP and VNN power bus lines are routed through a high-voltage optical relay with an enable line. The enable line can be used to cut power if voltages or currents are above specifications.

4) CCU App: The CCU communicates with the computer by opening a virtual serial port through a USB connection. Every command sent and received by the CCU has 64 bytes and includes authentication codes along with biasing and control commands. All the necessary codes and commands to communicate with the CCU are automatically generated with the CCU app, which is developed for Windows operating systems. The app monitors, programs, and controls the πCard system.

A companion app was also developed to help the user visualize the bias pattern being sent.

C. Short-Finding

To assist in finding and disabling shorted channels in fabricated TOBE arrays, a short finder script was written. The script loops through all channels defined for the transducer and the user is asked to decide if the channel is shorted or not. Usually, a channel is considered to have no shorts if the current drawn is less than 1 mA. Once the mapping procedure is finished, any shorted channels are set to a high-impedance state.

Fig. 11. Top: Hadamard transmit aperture encoding used in FORCES imaging scheme, showing a single row. Transmits sent along multiple rows are designed to effect a (steerable) elevation focus. Bias voltage polarity determines the transmit polarity in the electrostrictive material. The bias pattern is selected from a row or column of a Hadamard matrix. After each transmit event, data is received from every row, inverting the receive polarity when a negative bias is used. Bottom: Effective synthetic aperture imaging scheme after Hadamard aperture decoding.

D. Implementation of Real-Time FORCES Imaging

The combination of existing ultrasound systems with the πCard system can enable novel imaging schemes. One of the techniques to acquire high SNR images is to implement a FORCES imaging algorithm with TOBE arrays. Briefly, in the FORCES imaging scheme [9], a Hadamard bias pattern is applied on columns while a transmit pulse is applied to rows. Columns are used to receive the ultrasound signals. After every acquisition, an inverse Hadamard matrix is used to decode the

Fig. 12. Elevationally scanned (XZ plane) wire phantom using a 128 × 128 λ-pitch TOBE array and uFORCES. The wires are 25 μm in diameter.
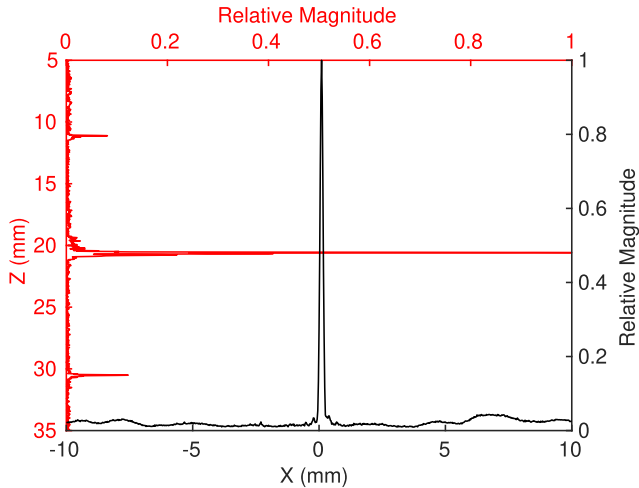

Fig. 13. Plot showing the axial and lateral spread of the 25 μm wires shown in Fig. 12. The red plot shows an axial resolution of 90 μm and the black plot shows a lateral resolution of 175 μm.

received signals to achieve an effective elevationally focused synthetic aperture dataset as shown in Fig. 11. Then delay and sum beamforming is performed to generate an ultrasound image for every sub-frame. Finally, a high-resolution image is formed by the summation of all the sub-frames. Cross-plane FORCES imaging performs the mentioned processes twice, once on rows and then on columns, by electronically switching the transmit, receive, and biasing channels. Volumetric 3-D imaging can be performed by electronically steering the imaging plane.

III. RESULTS

A. Test Results

The πCards were tested for variation by setting all output channels to a particular voltage and then measuring output on

each channel. This gave an average deviation of 0.032% across the four cards. Since this deviation is so small no additional consideration was given during imaging to correct for the difference in sensitivity between channels.

B. Pulse-Echo Measurements

A pulse-echo experiment was performed on a 128 × 128 array by immersing the transducer in water and placing an Aluminum block ≈5 mm from its surface. We treated each row and column as a single element and applied a bias of 80 V before applying a 20 Vpp transmit pulse. From the results we calculated an average center frequency of 13.5 MHz with a standard deviation of 1.79 MHz. Additionally, the average 6 dB fractional bandwidth of the elements was 36.8% with a standard deviation of 18.8%.

C. Crosstalk Measurements

Crosstalk can be broken down into two components: crosstalk from complimentary electronics and crosstalk between the transducer elements.

1) Crosstalk From Electronics: The system electronics were measured for crosstalk by connecting a function generator to one of the transducer output channels with the transducer absent from the system. The output function was a 300 mVpp 10 MHz sine wave. Data from all channels were acquired and normalized to the channel containing the signal. Nearest neighbors never exceeded −31 dB and next nearest neighbors never exceeded −36 dB. In the absence of our electronics the Verasonics system has a nearest neighbor crosstalk of −38 dB. We can conclude that our electronics contribute ≈7 dB of crosstalk to the system.

2) Crosstalk From the Transducer Elements: Now with a transducer connected we performed the same test. In this case the nearest neighbors never exceeded −28 dB relative to the channel with the signal. Therefore, the transducers contribute ≈3 dB of crosstalk. We expect this can be further improved in future work.

D. Real-Time FORCES Imaging

Using the previously developed FORCES imaging method [9] and a 128 × 128 TOBE array we obtained the wire phantom imaging result shown in Fig. 12. Here we achieved a lateral resolution of 175 μm and an axial resolution of 90 μm as shown in Fig. 13. We could perform cross-plane FORCES imaging at a rate of 20 frames/s and generate a movie of the target in real time.

E. 3-D Power Doppler Imaging

We sought to test our imaging platform's ability to achieve volumetric power Doppler imaging. We performed elevationally-scanned B-mode imaging using FORCES (for structure), while also performing Power-Doppler ultrasound imaging using elevationally focused plane-wave imaging (previously referred to as Scheme 1 [18]). Beamformed data from ten plane-wave excitations were wall-filtered and compounded to form a single Power Doppler 2-D image, and a set of

TABLE III
OBTAINED PARAMETERS COMPARED WITH EXISTING WORKS

Parameter	This Work	HV232 (Microchip) [25]	Row Driver in [26]	[27]	[28]
Peak to Peak Voltage	500Vpp	220Vpp	340Vpp	300V (positive only)	100V (positive only)
Transmit Voltage on Bias	190Vpp	0Vpp	N/A	N/A	N/A
Channel Count	256	8	256	16	1024
Rise Time	$32\mu s$	$5\mu s$	$13\mu s$	$8.56\mu s$	-
Fall Time	$35\mu s$	$5\mu s$	$5\mu s$	-	-
Total Peak Current	$\approx 2A$ (128 channels)	2A	100mA	-	$\approx 19mA$
Peak Current per Channel	$\approx 16mA$	10mA	N/A	0.4mA	$20\mu A$
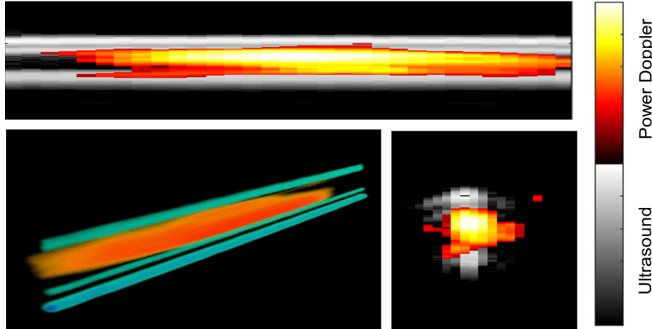
Fig. 14. 3-D power Doppler imaging of a flow phantom co-registered with ultrasound.
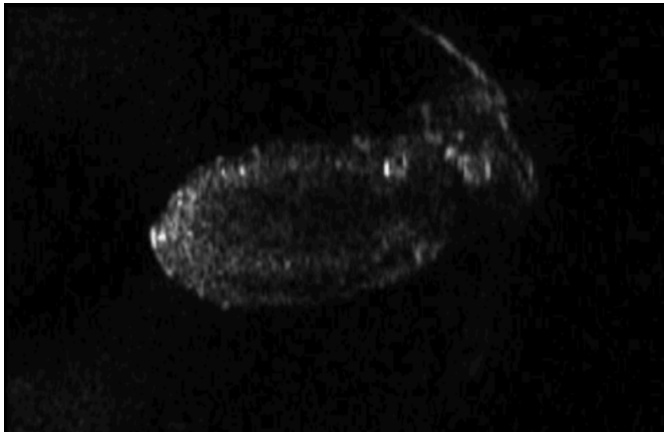
Fig. 15. Cross section of rat heart imaged with a 64 × 64 10 MHz TOBE Array. Video of fly-through is provided as ▦ supplementary material.

100 such images were acquired and rendered to form a 3-D Power Doppler image, with FORCES B-scans providing structural context. For a phantom, a corn starch solution (5g of cornstarch in 95 ml of deionized water) was passed through a plastic tube with a 0.5 mm diameter. Fig. 14 demonstrates the results of this experiment. We used a 64 × 64 electrostrictive TOBE transducer with a center frequency of 10 MHz.

F. Ex Vivo Tissue Imaging

To demonstrate the ability to image tissues with our system, we used a 64 × 64 TOBE array to image a rat heart ex vivo using elevationally scanned FORCES B-scan imaging. Fig. 15 shows one B-scan slice of the fly-through. The fly-through video is provided as ▦ supplementary material.

IV. DISCUSSION

Our current report is focused on a platform for tabletop evaluation of transducers. Future work should seek to develop more practical form factors for the transducers including handheld and wearable arrays designed for specific clinical applications. While the πCards themselves cannot currently be miniaturized, the IBs containing bias tees can be used to implement such handheld or wearable probes in future work. One powerful thing about our approach is the simplicity of the array. Our electronics could be coupled to multiple transducer form factors, with rapid development time for each transducer form-factor. Moreover, the transducers are simple enough to be wearable or scalable to large unprecedented arrays.

As shown in [7], there is potential for our technology to outperform matrix probes with microbeamformers. Our TOBE arrays can achieve synthetic aperture imaging with focusing in transmit and receive everywhere in-plane, while matrix probes often use weakly focused or unfocused transmissions and thus compromise resolution.

Currently, 10 kΩ resistors and 5.6 nF capacitors are used in bias tees. This gives an RC time constant of 56 μs. This is demonstrated by the C1V curve in Fig. 5(b). Thus, while the transducer switching times in Fig. 5(b) are in the 30 μs range, the switching times achieved when connected to the Verasonics Vantage system is slower, on the order of 120 μs. This should still enable pulse-repetition rates above 5 kHz and can enable ultrafast imaging applications. Future work should seek to improve this switching time for even faster rates.

While previous high-voltage drivers have been used in other fields such as liquid crystal displays (LCDs), MEMS devices (e.g., digital light processor (DLP) MEMs chips and MEMs switches) [25], [26], [27], [28], they have not achieved the high combined dc and transmit voltage and peak current requirements needed for our application. Table III summarizes the differences between our electronics and those cited.

The current electronics are configured for 256 channels, supporting a 128 × 128 TOBE array. However, the electronics are modular and expandable to 1024 channels, which could be pursued in future work. Note that the CCU currently has only four USB-C ports for πCard communication. To add more πCards (for more channels) we would need each USB-C port to have a splitter. In this way, 1024 channels can be supported, enabling future large 512 × 512 TOBE arrays.

In addition to ultrasound imaging work shown in this article, our technology will have future applicability to photoacoustic

imaging, since bias-encoded readout enables reception from every element of our TOBE arrays using only row–column addressing [19].

One problem still to be tackled is that of electrical safety. Our electronics generate sustained high voltages, which are absent in conventional ultrasound systems. While insulation and encapsulation should largely prevent macroshock issues, rapid switching of high voltages could be capacitively coupled through insulating matching layers to a subject. Thus grounding encapsulation is needed in future work and improved arrays incorporating these features are underway.

V. CONCLUSION

Here, a unique biasing electronics system was designed and developed for performing fast 3-D ultrasound imaging with bias-switchable TOBE arrays. Our πCard system can provide an arbitrary biasing sequence to a TOBE array to perform high-quality cross-plane B-scan and Power Doppler imaging. The πCard system can provide bipolar high-voltage bias voltages up to 500 V (or ±250 V) in approximately 100 μs. Live cross-plane FORCES and power Doppler ultrasound imaging were performed to experimentally test the advantages of bias-encoded imaging using the πCard system and TOBE arrays. Future work should optimize the fabrication of the TOBE arrays to prevent shorting and other problems. Improved imaging schemes for volumetric power Doppler and color Doppler imaging should also be explored. Future work should also aim to improve B-scan imaging frame rates with sparse synthetic aperture schemes. Finally, our ultrafast FORCES methods have the potential to outperform the state-of-the-art MATRIX probes with integrated micro-beamformers since our approach can achieve transmit and receive focusing everywhere in the scan plane, whereas MATRIX probes cannot [7]. Future work should further explore these opportunities.

DISCLOSURE

DATA SHARING

Data from this article may be provided upon request.

REFERENCES

[1] R. K. W. Chee, A. Sampaleanu, D. Rishi, and R. J. Zemp, "Top orthogonal to bottom electrode (TOBE) 2-D CMUT arrays for 3-D photoacoustic imaging," *IEEE Trans. Ultrason., Ferroelectr., Freq. Control*, vol. 61, no. 8, pp. 1393–1395, Aug. 2014.

[2] Q. Huang and Z. Zeng, "A review on real-time 3D ultrasound imaging technology," *BioMed Res. Int.*, vol. 2017, pp. 1–20, Mar. 2017.

[3] A. Fenster, J. Bax, H. Neshat, D. Cool, N. Kakani, and C. Romagnoli, "3D ultrasound imaging in image-guided intervention," in *Proc. 36th Annu. Int. Conf. IEEE Eng. Med. Biol. Soc.*, Aug. 2014, pp. 6151–6154.

[4] B. Savord and R. Solomon, "Fully sampled matrix transducer for real time 3D ultrasonic imaging," in *Proc. IEEE Symp. Ultrason.*, vol. 1, Oct. 2003, pp. 945–953.

[5] S. Blaak et al., "Design of a micro-beamformer for a 2D piezoelectric ultrasound transducer," in *Proc. IEEE Int. Ultrason. Symp.*, Sep. 2009, pp. 1338–1341.

[6] J. Janjic et al., "A 2-D ultrasound transducer with front-end ASIC and low cable count for 3-D forward-looking intravascular imaging: Performance and characterization," *IEEE Trans. Ultrason., Ferroelectr., Freq. control*, vol. 65, no. 10, pp. 1832–1844, Oct. 2018.

[7] M. R. Sobhani, M. Ghavami, A. K. Ilkhechi, J. Brown, and R. Zemp, "Ultrafast orthogonal row–column electronic scanning (uFORCES) with bias-switchable top-orthogonal-to-bottom electrode 2-D arrays," *IEEE Trans. Ultrason., Ferroelectr., Freq. Control*, vol. 69, no. 10, pp. 2823–2836, Oct. 2022.

[8] E. Roux, A. Ramalli, P. Tortoli, C. Cachard, M. Robini, and H. Liebgott, "2-D ultrasound sparse arrays multidepth radiation optimization using simulated annealing and spiral-array inspired energy functions," *IEEE Trans. Ultrason., Ferroelectr., Freq. Control*, vol. 63, no. 12, pp. 2138–2149, Dec. 2016.

[9] C. Ceroici, K. Latham, B. A. Greenlay, J. A. Brown, and R. J. Zemp, "Fast orthogonal row–column electronic scanning experiments and comparisons," *IEEE Trans. Ultrason., Ferroelectr., Freq. Control*, vol. 66, no. 6, pp. 1093–1101, Jun. 2019.

[10] D. H. Turnbull and F. S. Foster, "Beam steering with pulsed two-dimensional transducer arrays," *IEEE Trans. Ultrason., Ferroelectr., Freq. Control*, vol. 38, no. 4, pp. 320–333, Jul. 1991.

[11] R. E. Davidsen, J. A. Jensen, and S. W. Smith, "Two-dimensional random arrays for real time volumetric imaging," *Ultrason. Imag.*, vol. 16, no. 3, pp. 143–163, Jul. 1994.

[12] A. Ramalli, E. Boni, E. Roux, H. Liebgott, and P. Tortoli, "Design, implementation, and medical applications of 2-D ultrasound sparse arrays," *IEEE Trans. Ultrason., Ferroelectr., Freq. Control*, vol. 69, no. 10, pp. 2739–2755, Oct. 2022.

[13] M. Karaman, I. O. Wygant, Ö. Oralkan, and B. T. Khuri-Yakub, "Minimally redundant 2-D array designs for 3-D medical ultrasound imaging," *IEEE Trans. Med. Imag.*, vol. 28, no. 7, pp. 1051–1061, Jul. 2009.

[14] C. E. Morton and G. R. Lockwood, "Theoretical assessment of a crossed electrode 2-D array for 3-D imaging," in *Proc. IEEE Ultrason. Symp.*, vol. 1, Oct. 2003, pp. 968–971.

[15] N. M. Daher and J. T. Yen, "2-D array for 3-D ultrasound imaging using synthetic aperture techniques," *IEEE Trans. Ultrason., Ferroelectr., Freq. Control*, vol. 53, no. 5, pp. 912–924, May 2006.

[16] A. Sampaleanu, P. Zhang, A. Kshirsagar, W. Moussa, and R. J. Zemp, "Top-orthogonal-to-bottom-electrode (TOBE) CMUT arrays for 3-D ultrasound imaging," *IEEE Trans. Ultrason., Ferroelectr., Freq. Control*, vol. 61, no. 2, pp. 266–276, Feb. 2014.

[17] C. Ceroici, "Novel 3D ultrasound imaging techniques using top-orthogonal-to-bottom-electrode (TOBE) arrays," Ph.D. thesis, Univ. Alberta, Edmonton, AB, Canada, 2019, doi: 10.7939/r3-05bs-7730.

[18] C. Ceroici, T. Harrison, and R. J. Zemp, "Fast orthogonal row–column electronic scanning with top-orthogonal-to-bottom electrode arrays," *IEEE Trans. Ultrason., Ferroelectr., Freq. Control*, vol. 64, no. 6, pp. 1009–1014, Jun. 2017.

[19] C. Ceroici et al., "3D photoacoustic imaging using Hadamard-bias encoding with a crossed electrode relaxor array," *Opt. Lett.*, vol. 43, no. 14, pp. 3425–3428, 2018.

[20] K. Uchino, S. Nomura, L. E. Cross, R. E. Newnham, and S. J. Jang, "Electrostrictive effect in perovskites and its transducer applications," *J. Mater. Sci.*, vol. 16, no. 3, pp. 569–578, Mar. 1981.

[21] R. E. Davidsen and S. W. Smith, "Relaxor ferroelectric materials in two-dimensional transducer arrays," in *Proc. IEEE Ultrason. Symp., Int. Symp.*, vol. 2, 1995, pp. 1283–1286.

[22] A. K. Ilkhechi, C. Ceroici, Z. Li, and R. Zemp, "Transparent capacitive micromachined ultrasonic transducer (CMUT) arrays for real-time photoacoustic applications," *Opt. Exp.*, vol. 28, no. 9, pp. 13750–13760, 2020.

[23] M. Ghavami, A. K. Ilkhechi, and R. Zemp, "Flexible transparent CMUT arrays for photoacoustic tomography," *Opt. Exp.*, vol. 30, no. 10, pp. 15877–15894, May 2022.

[24] *Generic Standard on Printed Board Design*, Standard IPC-2221B, 2012.

[25] *Microchip, Low Charge Injection 8-Channel High Voltage Analog Switches With Bleed Resistors*, document HV232, datasheet, 2013.

[26] J. De Vos, H. De Smet, A. M. De Cubber, and A. Van Calster, "High-voltage CdSe-Ge TFT driver circuits for passive AC-TFEL displays," *IEEE J. Solid-State Circuits*, vol. 34, no. 2, pp. 228–232, Feb. 1999.

[27] J.-F. Saheb, J.-F. Richard, M. Sawan, R. Meingan, and Y. Savaria, "System integration of high voltage electrostatic MEMS actuators," *Analog Integr. Circuits Signal Process.*, vol. 53, no. 1, pp. 27–34, 2007.

[28] K. W. Current et al., "A high-voltage SOI CMOS exciter chip for a programmable fluidic processor system," *IEEE Trans. Biomed. Circuits Syst.*, vol. 1, no. 2, pp. 105–115, Jun. 2007.

Afshin Kashani Ilkhechi (Member, IEEE) was born in 1989. He received the B.Sc. degree in electronic engineering from the University of Tabriz, Tabriz, Iran, in 2012, the M.Sc. degree in electronic engineering from the Sahand University of Technology, Tabriz, in 2014, and the Ph.D. degree in biomedical engineering from the University of Alberta, Edmonton, AB, Canada, in 2022.

He is currently working on state-of-art biomedical devices to treat eye diseases mainly wet-stage age-related macular degeneration (AMD) and diabetic retinopathy. He is the author or a coauthor of numerous journal articles and conference papers in the field of microsystems and microelectromechanical systems and biomedical imaging technology.

Dr. Kashani Ilkhechi is also a reviewer of a number of journals and conferences in his fields of interest.

Randy Palamar (Graduate Student Member, IEEE) was born in High River, AB, Canada, in 1998. He received the B.Sc. degree (Hons.) in electrical engineering from the University of Alberta, Edmonton, AB, Canada, in 2022, where he is currently pursuing the M.Sc. degree as a member of the Dr. Zemp's Research Group, Department of Electrical and Computer Engineering.

His research interests include 4-D power Doppler imaging, functional ultrasound, and the design of high-voltage control electronics for novel beam-steering methods.

Mohammad Rahim Sobhani (Student Member, IEEE) was born in Tabriz, Iran. He received the B.Sc. degree (Hons.) in biomedical engineering (bio-electric) from the Sahand University of Technology, Tabriz, in 2012, and the M.Sc. degree in electrical and electronics engineering from Özyeğin University, Istanbul, Turkey, in 2015. He is currently pursuing the Ph.D. degree with the Department of Electrical and Computer Engineering, University of Alberta, Edmonton, AB, Canada.

He is currently a Graduate Assistant with the Department of Electrical and Computer Engineering, University of Alberta. His current research interests include the development of large-area top-orthogonal-to-bottom electrode arrays, transparent ultrasound transducers, and microfabrication.

Darren Dahunsi (Graduate Student Member, IEEE) was born in Ojo, Lagos, Nigeria, in 1998. He received the B.Sc. degree (Hons.) in engineering physics (nanoengineering) from the University of Alberta, Edmonton, AB, Canada, in 2021, where he is currently pursuing the Ph.D. degree as a member of the Dr. Zemp's Research Group, Department of Electrical and Computer Engineering.

His research interests include volumetric power Doppler imaging, ultrafast ultrasound beamforming, and real-time GPU computation.

Christopher Ceroici (Member, IEEE) received the B.Sc. degree in engineering physics from the University of Alberta, Edmonton, AB, Canada, in 2012, the M.Sc. degree in electrical engineering from the University of Waterloo, Waterloo, ON, Canada, in 2014, and the Ph.D. degree from the University of Alberta in 2019.

His research has focused on the fabrication and system integration of bias-sensitive ultrasound transducers.

Mahyar Ghavami (Student Member, IEEE) was born in Tabriz, Iran. He received the B.Sc. degree (Hons.) in mechanical engineering from the University of Tabriz, Tabriz, in 2014, and the M.Sc. degree (Hons.) in mechanical engineering from Tarbiat Modares University, Tehran, Iran, in 2017. He is currently pursuing the Ph.D. degree with the Dr. Zemp's Research Group, Department of Electrical and Computer Engineering, University of Alberta, Edmonton, AB, Canada.

His research interests focuses on the development of ultrasound transducers for biomedical applications. He is a holder of the Alberta Graduate Excellence Scholarship (AGES).
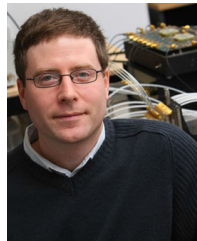
Jeremy Brown (Member, IEEE) was born in London, ON, Canada, in 1978. He received the B.Sc.Eng. degree in engineering physics and the Ph.D. degree in applied physics from Queen's University, Kingston, ON, Canada, in 2001 and 2005, respectively.

From 2006 to 2008, he was a Postdoctoral Researcher with the Sunnybrook Health Sciences Center, Toronto, ON, Canada. In 2008, he joined as a Faculty Member in biomedical engineering with Dalhousie University, Halifax, NS, Canada, where he is currently cross appointed to the Department of Electrical Engineering. In 2009, he joined the Department of Surgery, Nova Scotia Health Authority, Halifax, as the Affiliated Scientist. His research in high-frequency ultrasound is focused on the development of very high-resolution microfabricated imaging endoscopes for guided surgical applications and low-frequency ultrasound is focused on developing miniature highly focused therapeutic transducers for precision tissue ablation. His research interests include piezoelectric transducer design, fabrication, and characterization for both ultrasonic imaging and therapeutic applications and all of the associated electronic hardware required to drive capture, and process the ultrasonic signals.

Roger Zemp (Member, IEEE) was born in Calgary, AB, Canada, in 1974. He received the B.Sc. degree in physics from the University of Alberta, Edmonton, AB, Canada, in 1998, the M.A.Sc. degree in electrical and computer engineering from the University of Toronto, Toronto, ON, Canada, in 2000, and the Ph.D. degree in biomedical engineering from the University of California at Berkeley, Berkeley, CA, USA, in 2004.

From 2004 to 2006, he was with Texas A&M University, College Station, TX, USA, as a Postdoctoral Fellow, and then with Washington University, St. Louis, MO, USA, from 2006 to 2007. He is currently a Professor with the Department of Electrical and Computer Engineering, University of Alberta. His current research interests include ultrasound imaging, biomedical optics, and photoacoustic imaging.